Organic & Biomolecular Chemistry

PAPER

View Article Online
View Journal



Cite this: DOI: 10.1039/c6ob01734g

# Deoxyfluoro-D-trehalose (FDTre) analogues as potential PET probes for imaging mycobacterial infection†

Sarah R. Rundell,‡[a] Zachary L. Wagar,‡[a] Lisa M. Meints,[a] Claire D. Olson,[a] Mara K. O'Neill,[a] Brent F. Piligian,[a] Anne W. Poston,[a] Robin J. Hood,[a] Peter J. Woodruff[b] and Benjamin M. Swarts*[a]

*Mycobacterium tuberculosis*, the etiological agent of human tuberculosis, requires the non-mammalian disaccharide trehalose for growth and virulence. Recently, detectable trehalose analogues have gained attention as probes for studying trehalose metabolism and as potential diagnostic imaging agents for mycobacterial infections. Of particular interest are deoxy-[$^{18}$F]fluoro-D-trehalose ($^{18}$F-FDTre) analogues, which have been suggested as possible positron emission tomography (PET) probes for *in vivo* imaging of *M. tuberculosis* infection. Here, we report progress toward this objective, including the synthesis and conformational analysis of four non-radioactive deoxy-[$^{19}$F]fluoro-D-trehalose ($^{19}$F-FDTre) analogues, as well as evaluation of their uptake by *M. smegmatis*. The rapid synthesis and purification of several $^{19}$F-FDTre analogues was accomplished in high yield using a one-step chemoenzymatic method. Conformational analysis of the $^{19}$F-FDTre analogues using NMR and molecular modeling methods showed that fluorine substitution had a negligible effect on the conformation of the native disaccharide, suggesting that fluorinated analogues may be successfully recognized and processed by trehalose metabolic machinery in mycobacteria. To test this hypothesis and to evaluate a possible route for delivery of FDTre probes specifically to mycobacteria, we showed that $^{19}$F-FDTre analogues are actively imported into *M. smegmatis via* the trehalose-specific transporter SugABC-LpqY. Finally, to demonstrate the applicability of these results to the efficient preparation and use of short-lived $^{18}$F-FDTre PET radiotracers, we carried out $^{19}$F-FDTre synthesis, purification, and administration to *M. smegmatis* in 1 hour.

Received 16th June 2016,
Accepted 15th August 2016

DOI: 10.1039/c6ob01734g

www.rsc.org/obc

## Introduction

*Mycobacterium tuberculosis*, the organism that causes tuberculosis (TB), infects 2 billion people worldwide, every year causing 10 million active cases of TB and killing 1.5 million people.[1] Although drug-susceptible TB is curable, treatment requires multiple drugs delivered over the course of 6–9 months. Non-adherence to treatment has led to the emergence of multi- and extensively-drug-resistant TB (MDR- and XDR-TB), which are extremely difficult and costly to diagnose and treat.[2,3] In 2014, an estimated 5% of all new TB cases—nearly half a million—were MDR-TB, which had a case fatality rate approaching 50%.[4] To combat drug-susceptible and drug-resistant TB alike, new drugs and diagnostics—as well as new tools that support their development—are needed.

Nuclear imaging is emerging as a potentially transformative technology for TB research and clinical applications. As recently discussed by Johnson and co-authors, nuclear imaging modalities such as positron emission tomography (PET) may offer the ability to rapidly and noninvasively diagnose TB and monitor TB disease progression and response to treatment, while also allowing correlation of various disease characteristics with patient anatomy in real time and in three dimensions.[5] Thus, in principle, nuclear imaging can provide rich information on TB disease state that is complementary to diagnostic methods based on analysis of sputum samples by microscopy, culture, or nucleic acid detection.

[a]*Department of Chemistry and Biochemistry, Central Michigan University, Mount Pleasant, MI 48859, USA. E-mail: ben.swarts@cmich.edu*
[b]*Department of Chemistry, University of Southern Maine, Portland, ME, USA*
†Electronic supplementary information (ESI) available: Supplementary figures, experimental procedures, and NMR spectra. See DOI: 10.1039/c6ob01734g
‡These authors contributed equally to this work.

To date, nuclear imaging approaches for TB have primarily focused on the use of radiotracers that provide a readout of the host inflammatory response to infection. In particular, 2-deoxy-2-[$^{18}$F]fluoro-D-glucose ($^{18}$F-2-FDG) has been used extensively for PET imaging of inflammation associated with TB lesions.[5,6] However, $^{18}$F-2-FDG is not well-suited to differentiating TB from tumors and other metabolically active tissues due to non-specific uptake.[5,6] Radiolabeled analogues of antimycobacterial compounds, such as isoniazid, have been used for drug biodistribution studies,[7,8] and they may also have value for TB detection applications.[8] Radiotracers that specifically label bacteria may hold the most promise for *in vivo* imaging. Indeed, recent reports have demonstrated the potential of carbohydrate-based PET probes for imaging various types of bacterial infection,[9–11] but there has been limited progress for mycobacteria. Jain and co-workers imaged TB with 1-(2′-deoxy-2′-fluoro-beta-D-arabinofuranosyl)-5-[$^{125}$I]iodouracil ($^{125}$I-FIAU).[12] However, an engineered strain of *M. tuberculosis* expressing thymidine kinase was required to permit bacteria-selective uptake of $^{125}$I-FIAU, so this approach is limited to experimentally infected animals.[12] Therefore, as noted by Johnson and co-authors,[5] there is an urgent need for new mycobacteria-specific radiotracers that enable direct visualization of wild-type *M. tuberculosis* during infection.

Trehalose analogues modified with detectable tags have recently been explored as mycobacteria-specific imaging probes, and they are promising candidates for nuclear imaging applications. Trehalose (**1**) is a $C_2$-symmetric, non-mammalian disaccharide that is essential for mycobacterial growth and virulence due to its central role in cell wall biosynthesis.[13,14] Trehalose metabolic pathways that are conserved in mycobacteria are briefly discussed here to illustrate how they can be targeted for imaging probe development (Fig. 1). Biosynthesis of trehalose occurs from either glucose or polymeric α-glucan through metabolic cycles involving the enzymes OtsAB/trehalase or TreYZ/TreS, respectively.[15–17] Intracellular trehalose is converted by Pks13 to the glycolipid trehalose monomycolate (TMM),[18] which, upon translocation across the plasma membrane by MmpL3,[19–21] is utilized by the Ag85 complex to construct the mycobacterial outer membrane (also referred to as the mycomembrane).[22–24] Ag85 has a dual use for TMM, using it to generate: (i) arabinogalactan–mycolate (AGM), which is the foundation of the mycomembrane; and (ii) trehalose dimycolate (TDM), a mycomembrane-resident glycolipid which is involved in pathogenesis.[25–27] Free trehalose that is released during these Ag85-mediated processes is recycled back into the cell by the trehalose-specific transporter SugABC-LpqY.[28]

These pathways, which have only recently been fully elucidated, provide opportunities to rationally design trehalose-based probes for the detection of mycobacteria (Fig. 2A). The Barry and Davis groups reported the first trehalose-based imaging probe, a fluorescein-modified ketoside trehalose analogue (FITC-Tre, **2**), which was capable of metabolically labeling the mycobacterial cell wall *via* Ag85-mediated incorporation into trehalose glycolipids.[29] FITC-Tre was used to

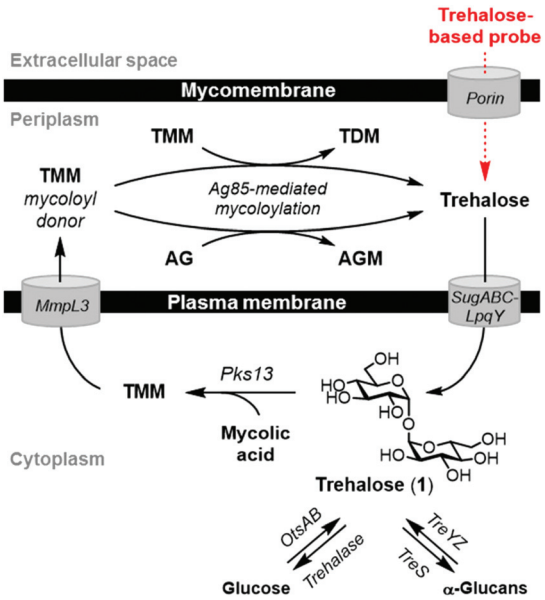


**Fig. 1** Conserved trehalose metabolic pathways in mycobacteria. Cytoplasmic trehalose (**1**) is converted to trehalose monomycolate (TMM), which is then exported and processed by the Ag85 complex to generate trehalose dimycolate (TDM) and arabinogalactan–mycolate (AGM). Released trehalose is recycled by SugABC-LpqY. Trehalose-based probes (red text) administered to mycobacteria can cross the mycomembrane, likely *via* a porin(s), and incorporate into the cell *via* SugABC-LpqY-mediated uptake and/or *via* Ag85-mediated incorporation into TMM, TDM, and/or AGM.

image live *M. tuberculosis* within an infected macrophage, showing the potential of trehalose-based probes for mycobacteria-specific imaging within the context of a mammalian host system.[29] Subsequently, the Bertozzi group reported a series of azide-modified trehalose (TreAz) analogues (**3–6**), all of which could be metabolically incorporated into trehalose glycolipids and subsequently detected by click chemistry reaction with alkyne-modified fluorophores.[30] Presumably due to the smaller size of the azide, three of the four reported TreAz analogues were taken up by the trehalose transporter SugABC-LpqY and incorporated into trehalose glycolipids *via* an intracellular route.[30] Our group recently developed a class of alkyne-modified TMM (AlkTMM) analogues (**7** and **8**), which could deliver alkyne-modified mycolic acid mimics to either TDM or AGM *via* the action of Ag85, thus tagging the lipid portions of these molecules.[31] Together, these studies revealed two routes by which trehalose-based probes can incorporate detectable tags into mycobacteria: (i) anchoring to the cell wall *via* periplasmic Ag85-mediated mycoloylation; (ii) accumulation in the cytoplasm *via* uptake through SugABC-LpqY, with possible downstream incorporation into trehalose glycolipids. FITC-Tre, TreAz, and AlkTMM analogues enabled cellular imaging and provided valuable information about targeting trehalose metabolic pathways, but their reliance on optical imaging for detection and, in the case of TreAz and AlkTMM analogues, a second-

 

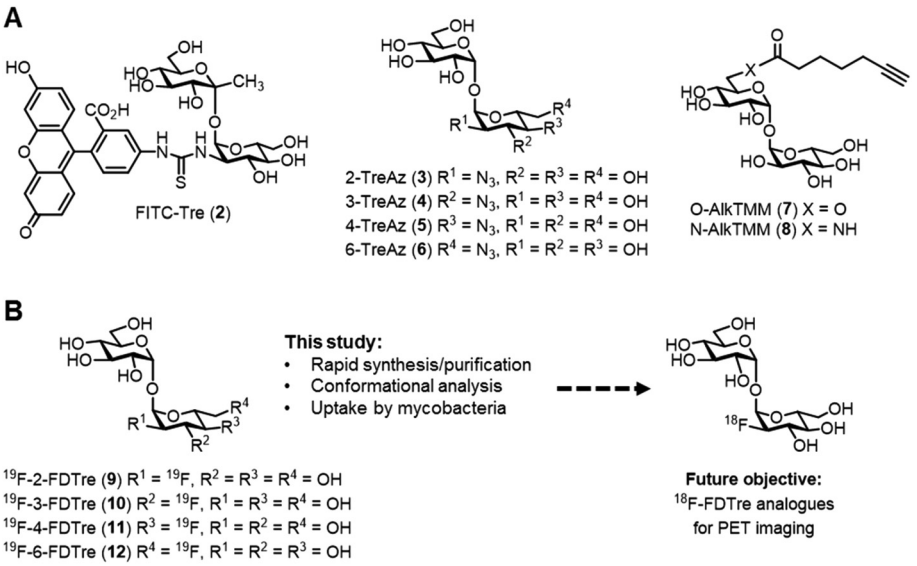


**Fig. 2** Trehalose-based probes for imaging mycobacteria. (A) Previously reported trehalose analogues modified with fluorescein (FITC-Tre) or click chemistry tags (TreAz and AlkTMM) have been used for optical imaging of intact mycobacterial cells. (B) This report describes the rapid synthesis, characterization, and mycobacterial uptake of non-radioactive deoxy-[$^{19}$F]fluoro-D-trehalose ($^{19}$F-FDTre) analogues **9–12**. This study informs the future development of radioactive deoxy-[$^{18}$F]fluoro-D-trehalose ($^{18}$F-FDTre) analogues for PET imaging.

ary labeling step, are not ideally suited to *in vivo* imaging applications.

The concept of a trehalose-based nuclear imaging probe was first introduced by Barry and Davis in 2011.[29] The most attractive candidate for this purpose would be a $^{18}$F-modified trehalose analogue, which, in principle, could be used for specific radiolabeling of wild-type *M. tuberculosis* within an infected host to allow *in vivo* PET imaging of TB. Two major challenges must be overcome to accomplish this objective. First, because $^{18}$F has a short half-life ($t_{1/2}$ = 110 min), the synthesis and purification of the $^{18}$F-labeled trehalose analogue must be rapid. Second, one or both of the mycobacteria-specific metabolic pathways discussed above (or perhaps as-yet undiscovered trehalose-related pathways) must be capable of incorporating the unnatural fluorine-modified trehalose analogue into live mycobacterial cells, *in vitro* and during host infection (*i.e.*, in a TB animal model or a human patient with TB). Herein, we present progress toward both of these goals. We report on the synthesis and conformational analysis of four non-radioactive deoxy-[$^{19}$F]fluoro-D-trehalose ($^{19}$F-FDTre) analogues (**9–12**, Fig. 2B), three of which were prepared using a rapid one-step chemoenzymatic method that is adaptable to the synthesis of radioactive deoxy-[$^{18}$F]fluoro-D-trehalose ($^{18}$F-FDTre) analogues. We also demonstrate that three of the four synthesized $^{19}$F-FDTre analogues were taken up by *M. smegmatis*, a model organism, *via* the SugABC-LpqY trehalose transporter, thus establishing a potential route for labeling of mycobacteria within a host organism. Together, these studies help to lay the groundwork for the future production and use of $^{18}$F-FDTre PET probes for *in vivo* TB imaging and potentially other applications.

## Synthetic approaches to FDTre analogues

Trehalose possesses $C_2$-symmetry and a 1,1-α,α-glycosidic bond, both of which present unique challenges to analogue synthesis. In general, one of two approaches is used to prepare trehalose analogues by chemical synthesis. For simpler targets, such as monofunctionalized analogues, trehalose desymmetrization and hydroxyl manipulation steps are typically used to modify the disaccharide. For more complex structures, for example sulfolipid analogues, specialized glycosylation methods have been developed to enable 1,1-α,α-stereoselective linkage of two properly functionalized glucose analogues. Although these approaches have been effectively applied to the synthesis of a variety of trehalose analogues, as recently reviewed by Kulkarni and co-workers,[32,33] they are often lengthy and low-yielding, and synthetic expertise is required for their execution.

A brief survey of prior chemical syntheses of FDTre analogues exemplifies these disadvantages. Of the $^{19}$F-FDTre analogues reported herein, only $^{19}$F-6-FDTre (**12**) has previously been chemically synthesized. In two independent reports, $^{19}$F-6-FDTre was accessed *via* trehalose desymmetrization strategies, which required 5 or 8 steps from trehalose and proceeded in 6 or 13% overall yield, respectively.[29,34] Critically, the final two-step fluorination–deprotection sequences in these syntheses had long reaction times (32–36 h) and moderate yields (39–48%).[29,34] In the same reports, syntheses with comparable lengths and yields were used to access an epimer of $^{19}$F-4-FDTre containing an axial fluoro group at the 4′-position.[29,34] Methyl ketoside derivatives of trehalose bearing

fluoro groups at the 2- and 3-positions have also been prepared[29] using established stereoselective glycosylation methods.[35–37] These approaches, while strategically elegant, are disadvantaged by incomplete 1,1-α,α-stereoselectivity, multiple protection and deprotection steps, and the use of custom monosaccharide building blocks. Overall, currently available methods for the chemical synthesis of trehalose analogues lack the speed, efficiency, and convenience desired for incorporating short-lived $^{18}$F into trehalose for PET applications.

Chemoenzymatic synthesis is an attractive alternative approach to preparing trehalose analogues, particularly if sensitive functionalities, such as radionuclides, must be quickly incorporated into the product. In principle, naturally occurring trehalose-synthesizing enzymes offer the ability to stereoselectively forge a 1,1-α,α-glycosidic bond between two unprotected glucose derivatives, thus bypassing the slow and inefficient chemical desymmetrization and glycosylation methods discussed above.[38] Ideally, an enzyme or series of enzymes would be capable of rapidly converting deoxy-[$^{18}$F]fluoro-D-glucose ($^{18}$F-FDG) analogues into $^{18}$F-FDTre analogues for PET imaging of mycobacterial infections. For example, $^{18}$F-2-FDG, which is commercially available and widely used in the clinic for PET imaging of tumors,[39] could be enzymatically transformed into $^{18}$F-2-FDTre for TB imaging applications.

In 2011, Barry and Davis reported the first chemoenzymatic synthesis of the non-radioactive version of $^{18}$F-2-FDTre, $^{19}$F-2-FDTre (**9**), using a three-enzyme system modeled after the OtsAB trehalose biosynthetic pathway in *Escherichia coli*.[29] The *E. coli* OtsAB pathway uses trehalose-6-phosphate synthase (OtsA) to catalyze a glycosylation reaction between glucose-6-phosphate and uridine diphosphate (UDP)-glucose, generating trehalose-6-phosphate, which is subsequently dephosphorylated by trehalose-6-phosphate phosphatase (OtsB) to give trehalose.[40,41] In adapting this pathway to the laboratory synthesis of $^{19}$F-2-FDTre, the authors used yeast hexokinase to first transform $^{19}$F-2-FDG into $^{19}$F-2-FDG-6-phosphate, which was then processed sequentially by OtsA and alkaline phosphatase (in lieu of OtsB) to give $^{19}$F-2-FDTre (**9**).[29] This work established the concept of using enzymes to access a FDTre analogue from the corresponding FDG analogue and should be adaptable to the synthesis of $^{18}$F-2-FDTre from $^{18}$F-2-FDG. However, in addition to being applied to only a single reaction example, this approach is limited by the need for three enzymatic steps, the inability to use 6-position-modified glucose substrates, and the use of overnight reactions.

In 2014, we reported a one-step chemoenzymatic method for the synthesis of trehalose analogues that addressed many of the limitations discussed above.[42] Our method exploited the unidirectional trehalose biosynthetic pathway in *Thermoproteus tenax*, which is a hyperthermophilic bacterium that utilizes a trehalose synthase (TreT) enzyme to catalyze the direct formation of trehalose from glucose and UDP-glucose (reaction scheme shown in Fig. 3A).[43] We showed that recombinant *T. tenax* TreT, which was expressed and purified from *E. coli*, could tolerate a variety of different glucose analogues (*e.g.*, azido, deoxy, fluoro, and stereochemical modifications),

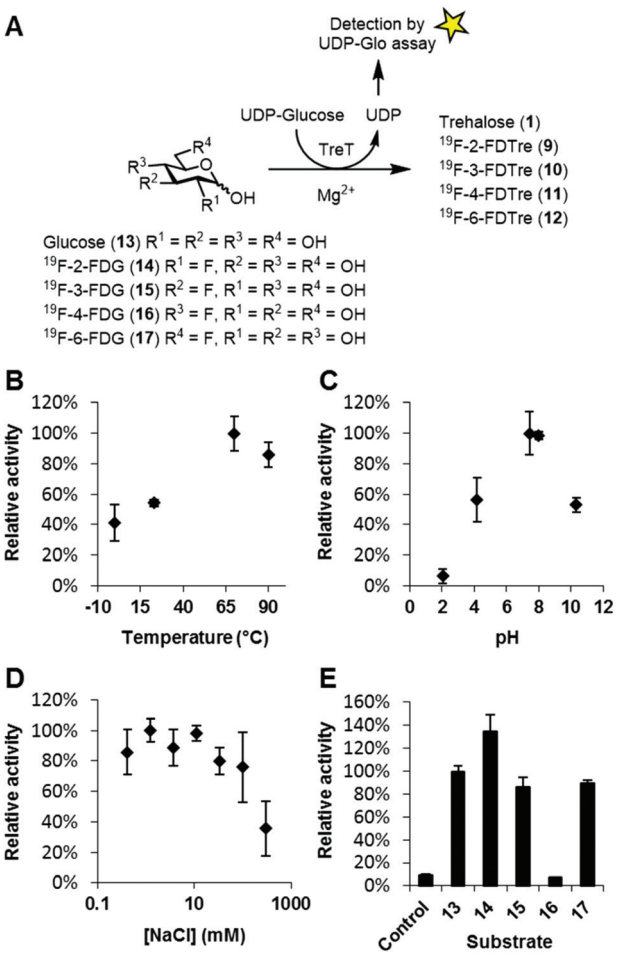


**Fig. 3** Optimization of TreT activity for FDTre synthesis. (A) Scheme for TreT-catalyzed one-step synthesis of $^{19}$F-FDTre analogues from $^{19}$F-FDG analogues. A luminescence-based UDP detection assay was used to assess enzyme activity during reaction optimization and substrate testing. Relative enzyme activity was assessed for varying (B) temperature, (C) pH, (D) salt concentration, and (E) substrate. Reactions were performed with 1 μg TreT at 23 °C in 50 mM Tris-HCl buffer, 10 mM acceptor substrate, 0.4 mM UDP-glucose, 20 mM $MgCl_2$, and 200 mM NaCl, unless noted otherwise. For pH dependence experiments, the following buffers were used: pH 2, sodium citrate; pH 4 sodium acetate, pH 7.4, sodium phosphate; pH, 8 Tris-HCl; pH 10, sodium carbonate.

generating the corresponding trehalose analogues quickly (60 min) and in high yield (up to >99%, as determined by HPLC) in a single step.[42] Because this reaction exhibited promising preliminary results on $^{19}$F-FDG substrates and possessed high efficiency, substrate flexibility, and speed, we reasoned that it would be an ideal platform for the development of $^{18}$F-FDTre PET imaging probes.

## Results and discussion

### Optimization of TreT activity for $^{19}$F-FDTre synthesis

In our previous report,[42] four commercial $^{19}$F-FDG analogues were screened as substrates for *T. tenax* TreT. Microscale

 

enzymatic reactions (50 μL) were performed in 50 mM HEPES buffer (pH 7.4) using 10 μM TreT, 10 mM $^{19}$F-FDG, 40 mM UDP-glucose, 300 mM NaCl, and 20 mM $MgCl_2$, with incubation and shaking at 70 °C for 60 min. After quenching with cold acetone, an HPLC assay employing an aminopropyl analytical column and refractive index detection was used to determine reaction yields. Complete conversion of $^{19}$F-2-, $^{19}$F-3-, and $^{19}$F-6-FDG analogues to the corresponding $^{19}$F-FDTre analogues was observed, whereas the $^{19}$F-4-FDG reaction did not proceed appreciably under the conditions tested (nor did other glucose analogues with modifications at the 4-position, likely due to a strict requirement for an equatorial hydroxyl group at this site). Based on these promising preliminary results, here we sought to optimize the TreT reaction for the production of FDTre analogues. To facilitate these efforts, we replaced the slow, low-sensitivity HPLC assay with a rapid and sensitive luminescence-based glycosytransferase assay. This assay, which detects UDP released from the UDP-sugar donor upon reaction, was used to optimize TreT reaction conditions and assess relative enzyme activities on $^{19}$F-FDG substrates.

Using the natural substrates glucose (**13**) and UDP-glucose, the luminescence assay was used to evaluate the dependence of TreT activity on temperature, pH, buffer, and NaCl concentration (Fig. 3A–D). The growth temperature for *T. tenax* in its native environment is 86 °C and TreT is heat-stable,[43] so it was not surprising that an elevated reaction temperature of 70 °C was optimal for TreT activity (Fig. 3B). High enzyme activity was also observed at 90 °C, which allows for the use of TreT at higher temperatures to decrease reaction times if needed. Different buffers spanning a range of pH values (2–10.4) were also tested (Fig. 3C). With the highest activity occurring at pH 7–8, pH 8.0 was chosen since it appeared to provide better protein stability during storage. At pH 7–8, the enzyme had comparable activity in various buffers, including HEPES, sodium phosphate, and Tris-HCl. We used 50 mM Tris-HCl due to its easy removal during product purification. According to the luminescence assay, TreT activity decreased as NaCl concentration increased above 100 mM (Fig. 3D). However, we did not observe significantly lower reaction conversions in high salt conditions by HPLC or TLC,§ and low salt conditions led to protein precipitation. Therefore, NaCl was maintained at 300 mM to achieve a balance between enzyme activity and stability.

Next, the relative activities of TreT on $^{19}$F-FDG analogues (**14**–**17**) relative to the natural acceptor glucose (**13**) were determined using the luminescence assay (Fig. 3E). Consistent with the reaction yields obtained from our earlier HPLC assay, the luminescence assay showed that TreT had high activity on $^{19}$F-2-, $^{19}$F-3-, and $^{19}$F-6-FDG. Surprisingly, $^{19}$F-2-FDG appeared to be a better substrate for TreT than glucose, with a relative activity of 135 ± 14%. This result is of significance because, as mentioned above, $^{18}$F-2-FDG is a widely used and commercially available PET imaging agent that could be readily converted by TreT to $^{18}$F-2-FDTre for PET imaging applications. $^{19}$F-3- and $^{19}$F-6-FDG also showed high activities of 86 ± 9% and 89 ± 3%, respectively. Although $^{18}$F-3- and $^{18}$F-6-FDG are not commercially available, their radiosyntheses have been reported,[44,45] so it would be feasible to converge these methods with the TreT reaction to access radioactive $^{18}$F-3- and $^{18}$F-6-FDTre chemoenzymatically. $^{19}$F-4-FDG showed no activity in this assay, confirming that chemoenzymatic synthesis of $^{19}$F-4-FDTre using wild-type *T. tenax* TreT is not achievable.

### Synthesis and purification of $^{19}$F-FDTre analogues

With TreT's substrate tolerance for $^{19}$F-FDG analogues established and with some reaction parameters optimized, we proceeded to the synthesis of $^{19}$F-FDTre analogues (Fig. 4). $^{19}$F-2-, $^{19}$F-3-, and $^{19}$F-6-FDTre (**9**, **10**, and **12**) were prepared by enzymatic synthesis from the corresponding commercially available $^{19}$F-FDG analogues (**14**, **15**, and **17**) (Fig. 1A). The enzymatic reactions were performed on a larger scale (4 mL) in 50 mM Tris-HCl buffer (pH 8.0) using 10 μM TreT, 300 mM

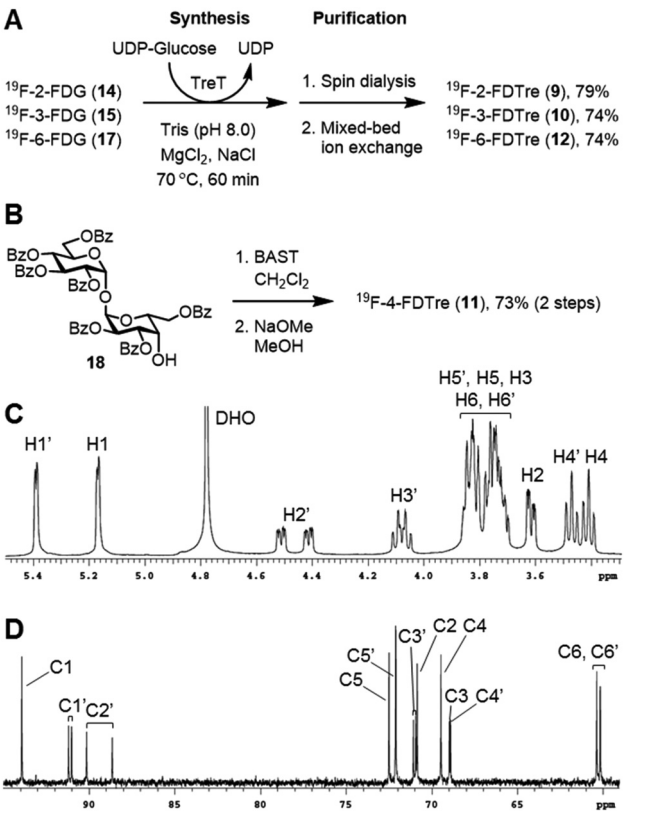


Fig. 4 (A) TreT-catalyzed chemoenzymatic synthesis and purification of $^{19}$F-2-, $^{19}$F-3-, and $^{19}$F-6-FDTre (**9**, **10**, and **12**) on a semi-preparative scale. Isolated yields following spin dialysis and ion exchange purification steps are shown. (B) Chemical synthesis of $^{19}$F-4-FDTre (**11**). Representative (C) $^{1}$H and (D) $^{13}$C NMR spectra for $^{19}$F-2-FDTre (see ESI† for all spectra).

§ The observed decrease in luminescence signal at higher NaCl concentrations is likely not due to decreased TreT activity, but instead due to effects on the coupled luciferase reaction. The assay manufacturer recommends maintaining NaCl at ≤200 mM.

NaCl, and 20 mM $MgCl_2$. During reaction optimization, we also noted that a 1 : 2 ratio of $^{19}$F-FDG : UDP-glucose gave yields similar to the previously used 1 : 4 ratio. Therefore, reactions were carried out using 20 mM $^{19}$F-FDG and 40 mM UDP-glucose, with incubation and shaking at 70 °C for 60 min. TLC analysis of the reactions showed complete conversion of each $^{19}$F-FDG analogue to the corresponding $^{19}$F-FDTre analogue.

Bearing in mind the speed needed for future production of radioactive $^{18}$F-FDTre, we developed a rapid and straightforward method to isolate $^{19}$F-FDTre analogues from crude enzymatic mixture. First, the TreT enzyme was removed *via* spin dialysis employing a 10 kDa molecular weight cutoff (MWCO) centrifugal filter unit. Next, the aqueous filtrate was treated with mixed-bed ion exchange resin to remove all ionic species, leaving only the neutral $^{19}$F-FDTre product in aqueous solution after filtration of the resin beads. Using this protocol, $^{19}$F-2-, $^{19}$F-3-, and $^{19}$F-6-FDTre were isolated in yields of 79%, 74%, and 74%, respectively, each on a ~20 mg scale. Given that complete reaction conversion was observed by TLC, it is likely that the loss of product was due to some binding of $^{19}$F-FDTre product to the resin beads. NMR and ESI-MS were used to characterize the $^{19}$F-FDTre products (representative $^1$H and $^{13}$C NMR data are shown for $^{19}$F-2-FDTre in Fig. 4C and D). The anomeric $^3J_{HH}$ coupling constants of all three enzymatically synthesized $^{19}$F-FDTre analogues ranged from 3.5–4.0 Hz, which established 1,1-α,α stereochemistry of the newly formed glycosidic bonds. Additionally, $^1$H and $^{19}$F NMR spectra exhibited the expected peak characteristics for the fluorinated position of each analogue. Together, the one-step synthesis and ion exchange purification procedures are convenient and fast, occurring on a timescale that is sufficient for $^{18}$F-FDTre synthesis (demonstrated in the section "Protocol for the rapid synthesis, purification, and administration of $^{19}$F-2-FDTre to *M. smegmatis* as a model for future $^{18}$F-FDTre PET imaging applications").

Although $^{19}$F-4-FDTre was not accessible through chemoenzymatic synthesis with wild-type *T. tenax* TreT, we decided to synthesize it chemically so that all four monofluorinated trehalose analogues could be systematically evaluated in conformational studies and bacterial uptake experiments (Fig. 4B). To initiate the synthesis, known trehalose heptabenzoate derivative **18**,[46] bearing a free axial 4-position OH group, was prepared *via* a reported route requiring 3 steps from trehalose. Bis(2-methoxyethyl)aminosulfur trifluoride (BAST) was used to fluorinate the free 4′-position of **18** with inversion of stereochemical configuration, which was followed by NaOMe-mediated debenzoylation to give $^{19}$F-4-FDTre (**11**) in 73% yield from **18** over two steps. $^1$H NMR spectroscopic analysis of $^{19}$F-4-FDTre showed H4′ chemical shift ($\delta$ 4.36 ppm), splitting pattern (doublet of triplets), and coupling constants ($^3J_{HH}$ = 9.5 Hz, $^2J_{HF}$ = 51.5 Hz) that were consistent with the presence of an equatorial fluorine atom at the 4′-position.

### Conformational analysis of $^{19}$F-FDTre analogues

The success of $^{18}$F-FDTre analogues as mycobacteria-specific PET imaging probes will depend on their ability to mimic native trehalose within the environment of the mycobacterium. Therefore, minimal distortion of the trehalose structure upon deoxyfluorination is desired for this application. While substitution of a hydroxyl group with a smaller fluorine atom does not have a notable steric impact, the higher electronegativity of fluorine *versus* oxygen, as well as its inability to act as a hydrogen bond donor, have the potential to modulate sugar structure and function. To provide insight into the effect of monodeoxyfluorination on the structure of trehalose, we used NMR and molecular modeling to define and compare the solution conformations of unmodified trehalose and the four synthesized $^{19}$F-FDTre analogues.

The structure of native trehalose has been investigated extensively due to its biological importance and applications in biopreservation. Experimental studies have primarily focused on establishing trehalose's solution conformation using NMR-derived intra- and inter-residue dihedral angles, most importantly those around the glycosidic bond, $\varphi_H$ (H1–C1–O1–C1′) and $\psi_H$ (C1–O1–C1′–H1′) (see Fig. 5 for $\varphi_H$ and $\psi_H$ definitions). When interpreted through Karplus curves, vicinal $^3J_{HH}$ coupling constants provide intra-residue dihedral angles, whereas long-range heteronuclear $^3J_{COCH}$ coupling constants provide the glycosidic dihedral angles $\varphi_H$ and $\psi_H$. An early NMR study of trehalose provided $^3J_{HH}$ coupling constants that clearly established $^4C_1$ chair conformations for the identical glucopyranoside rings.[47] Before suitable NMR techniques were available, experimental values for $\varphi_H$ and $\psi_H$ were obtained from X-ray crystallographic analysis of trehalose dihydrate ($\varphi_H$ = −41°, $\psi_H$ = −58°)[48] and anhydrous trehalose ($\varphi_H$ = −60°, $\psi_H$ = −59°),[49] as well as from optical rotation studies of trehalose in solution ($\varphi_H$ = $\psi_H$ = −60°).[50] Later on, several groups used NMR techniques to extract trehalose's glycosidic $^3J_{COCH}$ coupling constants, which were converted to $\varphi_H$ and $\psi_H$ values using a Karplus-type correlation curve developed by Tvaroška and co-workers (eqn (1)).[51]

$$^3J_{COCH} = 5.7\cos^2(\theta) - 0.6\cos(\theta) + 0.5 \quad (1)$$

Using this approach, the groups of Batta ($^3J_{COCH}$ = 3.3 Hz; $\varphi_H$ = $\psi_H$ = −41°),[52] Jiménez-Barbero ($^3J_{COCH}$ = 3.0 Hz; $\varphi_H$ = $\psi_H$ =

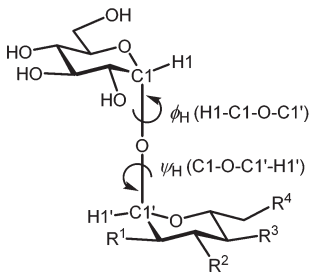


Trehalose (**1**) $R^1 = R^2 = R^3 = R^4 = OH$
$^{19}$F-2-FDTre (**9**) $R^1 = {}^{19}F$, $R^2 = R^3 = R^4 = OH$
$^{19}$F-3-FDTre (**10**) $R^2 = {}^{19}F$, $R^1 = R^3 = R^4 = OH$
$^{19}$F-4-FDTre (**11**) $R^3 = {}^{19}F$, $R^1 = R^2 = R^4 = OH$
$^{19}$F-6-FDTre (**12**) $R^4 = {}^{19}F$, $R^1 = R^2 = R^3 = OH$

**Fig. 5** Definition of the glycosidic dihedral angles $\varphi_H$ and $\psi_H$ for trehalose and $^{19}$F-FDTre analogues.

 

Table 1 Experimental[a] and theoretical glycosidic dihedral angles for trehalose and $^{19}$F-FDTre analogues

| | Experimental values[a] | | Theoretical values | | |
|---|---|---|---|---|---|
| Compound | $\varphi_H$ [b]; $^3J_{COCH}$ | $\psi_H$ [b]; $^3J_{COCH}$ | $\varphi_H$; $^3J_{COCH}$ [b] | $\psi_H$; $^3J_{COCH}$ [b] | Ref. |
| Trehalose (**1**) | −41°; 3.3 Hz | −41°; 3.3 Hz | | | 49 |
| | −44°; 3.0 Hz | −44°; 3.0 Hz | −50°; 2.5 Hz | −50°; 2.5 Hz | 50 |
| | −42°; 3.2 Hz | −42°; 3.2 Hz | −38°; 3.6 Hz | −38°; 3.6 Hz | 51 |
| | | | −50°; 2.5 Hz | −50°; 2.5 Hz | 44 |
| | | | −45°; 2.9 Hz | −45°; 2.9 Hz | 52 |
| | | | −54°; 2.1 Hz | −54°; 2.1 Hz | 53 |
| | | | −45°; 2.9 Hz | −45°; 2.9 Hz | 54 |
| | −44°; 3.0 Hz | −44°; 3.0 Hz | −52°; 2.3 Hz | −52°; 2.3 Hz | [c] |
| $^{19}$F-2-FDTre (**9**) | −41°; 3.3 Hz | −40°; 3.4 Hz | −52°; 2.3 Hz | −52°; 2.3 Hz | [c] |
| $^{19}$F-3-FDTre (**10**) | −43°; 3.1 Hz | −41°; 3.3 Hz | −52°; 2.3 Hz | −52°; 2.3 Hz | [c] |
| $^{19}$F-4-FDTre (**11**) | −44°; 3.0 Hz | −44°; 3.0 Hz | −51°; 2.4 Hz | −51°; 2.4 Hz | [c] |
| $^{19}$F-6-FDTre (**12**) | −43°; 3.1 Hz | −42°; 3.2 Hz | −52°; 2.3 Hz | −52°; 2.3 Hz | [c] |

[a] Only NMR-determined values are shown. [b] Calculated using the Karplus equation of Tvaroška (eqn (1)).[51] [c] This study.

−44°),[53] and Cheetham ($^3J_{COCH}$ = 3.2 Hz; $\varphi_H = \psi_H$ = −42°)[54] obtained results that were in close agreement (Table 1). In addition, theoretical values for $\varphi_H$ and $\psi_H$ of trehalose, calculated using various computational methods, ranged from −38° to −54° (Table 1).[47,52,53,55–57] Altogether, the experimental and theoretical studies were generally in good accord with one another, and indicated that trehalose has a relatively rigid structure in aqueous solution.

Based on the relatively inflexible nature of trehalose, coupled with the negligible effect deoxygenation has on its structure,[58,59] we predicted that monodeoxyfluorination would not have a major impact on its conformation. This hypothesis was supported by a simple conformational search employing the MM3* force field,[60] which predicted tightly grouped $\varphi_H$ and $\psi_H$ values (−51° to −52°) for the lowest energy conformers of trehalose and the four FDTre analogues (Table 1). A superposition of the five MM3*-derived theoretical structures, shown in Fig. 6A, depicts their similarity.

NMR spectroscopy was used to experimentally determine the analogues' solution conformations. $^1$H, $^{13}$C, COSY, and HSQC NMR spectra were acquired and analyzed to make resonance assignments for each compound. Analysis of vicinal $^3J_{HH}$ values confirmed that the $^4C_1$ chair conformations of the hexose rings were not distorted by fluorine substitution. To determine the long-range $^3J_{COCH}$ coupling constants across the glycosidic bond, we performed a 2D excitation-sculptured indirect-detection NMR experiment (EXSIDE)[61] with anomeric proton(s) selected (H1 for trehalose; H1 and H1′ for the $^{19}$F-FDTre analogues). The dihedral angles $\varphi_H$ and $\psi_H$ were then calculated using Tvaroška's Karplus-type equation shown above (eqn (1)).[51] Representative EXSIDE spectra for trehalose and $^{19}$F-2-FDTre are shown in Fig. 6C and D, respectively (see Fig. S1 in the ESI† for all EXSIDE spectra).

For native trehalose, the $^3J_{COCH}$ constant and corresponding glycosidic bond dihedral angles ($^3J_{COCH}$ = 3.0 Hz; $\varphi_H = \psi_H$ = −44°) were in excellent agreement with previously reported data (Table 1). For the $^{19}$F-FDTre analogues, the $^3J_{COCH}$ constants spanned 3.0–3.4 Hz, which corresponded to $\varphi_H$ and $\psi_H$ values ranging from −40 to −45° (Table 1). These values fall well within the $\varphi_H$ and $\psi_H$ ranges for unmodified trehalose that were established earlier by others and confirmed by our group in this study. Applying the experimentally determined $\varphi_H$ and $\psi_H$ dihedral angles as constraints, the lowest energy conformers of trehalose and the $^{19}$F-FDTre analogues were recalculated using MM3* and presented as a superposition in Fig. 6B. Taken together, the NMR and modeling data presented here demonstrate that monodeoxyfluorination has little impact on the solution conformation of trehalose, suggesting that components of mycobacterial trehalose metabolism may recognize and process FDTre analogues similarly to trehalose.

### Uptake of $^{19}$F-FDTre analogues by *M. smegmatis*

After confirming that FDTre analogues faithfully mimic the solution structure of trehalose, we tested their uptake in *M. smegmatis*, a frequently used avirulent model organism for *M. tuberculosis*. As discussed in the introduction, mycobacteria possess at least two conserved, mycobacteria-specific pathways through which FDTre analogues could accumulate in the cell: (i) extracellular Ag85-mediated mycoloylation to anchor FDTre to the cell wall; (ii) SugABC-LpqY-mediated uptake into the cytoplasm, possibly followed by incorporation into cell-wall trehalose glycolipids. While no cellular uptake experiments have been reported for FDTre analogues, it was previously shown that $^{19}$F-2-FDTre (**9**) reacted with a TDM analogue *in vitro* in the presence of recombinant Ag85.[29] However, Ag85 operates in the opposite direction *in vivo*, converting two molecules of TMM to one molecule each of TDM and trehalose, the latter of which is recycled back into the cell (see Fig. 1).[28] Therefore, it is possible that Ag85-catalyzed mycoloylation of FDTre analogues would not occur appreciably in living cells, unless a high concentration of the analogue were available in the periplasm to force the reverse reaction.

Previous cellular labeling experiments with TreAz analogues suggest that the trehalose recycling route may provide efficient uptake of FDTre analogues by mycobacteria. SugABC-LpqY is constitutively expressed and required for virulence of *M. tuberculosis*, and its function *in vivo* is to import free trehalose that is released by Ag85-catalyzed mycoloylation

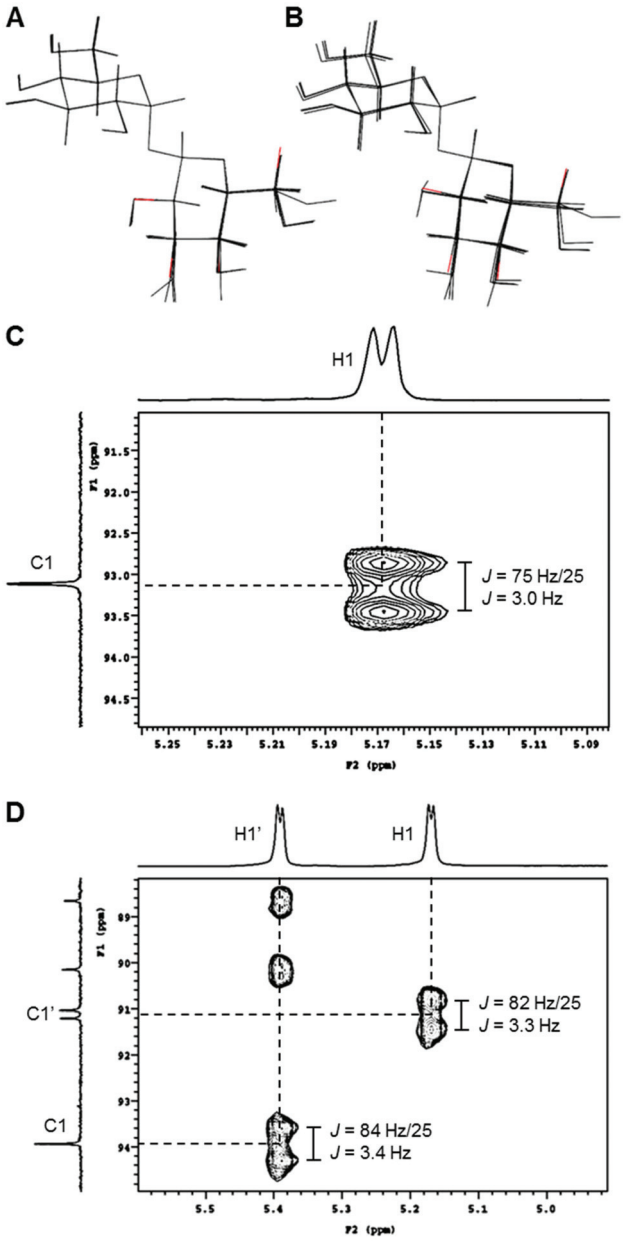


**Fig. 6** Conformational analysis of trehalose and $^{19}$F-FDTre analogues. Superpositions of the lowest energy conformers of trehalose and $^{19}$F-FDTre analogues (**1**, **9**–**12**) determined by conformational searches using MM3* (A) without constraints and (B) with NMR-determined $\varphi_H$ and $\psi_H$ values as constraints. The fluorine atom of each $^{19}$F-FDTre structure is colored red. Representative EXSIDE spectra are shown for (C) trehalose (**1**) and (D) $^{19}$F-2-FDTre (**9**). $^3J_{COCH}$ values were measured from EXSIDE spectra using a scaling factor of 25, as shown. See Fig. S1 and S2 in the ESI† for additional EXSIDE spectra and structural images for all compounds.

processes.[28] Although SugABC-LpqY is known to be highly specific for α,α-trehalose *versus* other disaccharides (*e.g.*, α,β-trehalose and maltose),[28] the Bertozzi group demonstrated that 2- and 6-TreAz (**3** and **6**) were actively imported into the cell by SugABC-LpqY and subsequently incorporated into trehalose glycolipids at relatively low concentrations (25 μM) in both *M. smegmatis* and *M. bovis* BCG.[30] On the other hand, 3-TreAz (**4**), which also labeled the cell surface, was not taken up by SugABC-LpqY in either species.[30] Instead, it was presumably anchored to the cell wall *via* periplasmic Ag85-mediated mycoloylation. A much higher concentration of 3-TreAz (500 μM) was required to achieve labeling, and even then it was only about 10–20% of the surface labeling given by a much lower concentration of 2- and 6-TreAz (25 μM).[30] 4-TreAz (**5**) was also taken up by SugABC-LpqY in *M. smegmatis*, though not in *M. bovis* BCG.[30] These studies indicated that SugABC-LpqY is tolerant of some trehalose analogues bearing small hydroxyl replacement modifications, and that it may incorporate such analogues into mycobacterial cells more efficiently than Ag85.¶ Based on these data, we hypothesized that subtly modified FDTre analogues would undergo SugABC-LpqY-mediated transport into mycobacteria.

We evaluated the four $^{19}$F-FDTre analogues synthesized in this study for SugABC-LpqY-mediated uptake into whole cells of *M. smegmatis*. To determine whether uptake was passive or dependent on the trehalose transporter SugABC-LpqY, three bacterial strains were tested in parallel: (i) *M. smegmatis* wild type; (ii) *M. smegmatis ΔsugC* mutant, which lacked a functional SugABC-LpqY transporter; and (iii) *M. smegmatis ΔsugC*::*sugC* complement, which had the transporter restored.[42] Each strain was cultured in the presence of 25 μM $^{19}$F-FDTre or left untreated, then cells were washed and lysed. Cytosolic extracts containing water-soluble species were dried and subjected to trimethylsilyl (TMS) derivatization using *N*-methyl-*N*-(trimethylsilyl) trifluoroacetamide (MSTFA). TMS-derivatized extracts were analyzed by GC-MS to provide a qualitative assessment of $^{19}$F-FDTre uptake (Fig. 7 shows representative GC-MS data for $^{19}$F-2-FDTre; see Fig. S3 in the ESI† for data on other analogues).

As expected, all cytosolic extracts contained a prominent peak for native trehalose, which is endogenously biosynthesized in the cytoplasm as described in the introduction. For samples that were treated with $^{19}$F-2-, $^{19}$F-3-, and $^{19}$F-6-FDTre (**9**, **10**, and **12**), the corresponding FDTre peaks were observed in wild-type *M. smegmatis* but not in the untreated controls, indicating that these analogues entered the cell. Critically, the FDTre peaks were absent in the *M. smegmatis ΔsugC* mutant and restored in the *M. smegmatis ΔsugC*::*sugC* complement, which confirmed that SugABC-LpqY was solely responsible for the observed analogue uptake. By contrast, $^{19}$F-4-FDTre (**11**) was not taken up by *M. smegmatis*.

Between the TreAz and FDTre uptake experiments, it can be concluded that small 2- and 6-position monosubstitutions are fairly well-tolerated by SugABC-LpqY in *M. smegmatis*. Because 4-TreAz and $^{19}$F-3-FDTre were taken up by SugABC-LpqY but 3-TreAz and $^{19}$F-4-FDTre were not, there appears to be mixed

¶Ag85 may be involved in FDTre labeling at lower probe concentrations, most likely through the following pathway: SugABC-LpqY-mediated uptake followed by Pks13-catalyzed mycoloylation to form fluorine-modified TMM, which would then undergo MmpL3-mediated export and further mycoloylation by Ag85 to give fluorine-modified TDM (refer to Fig. 1).

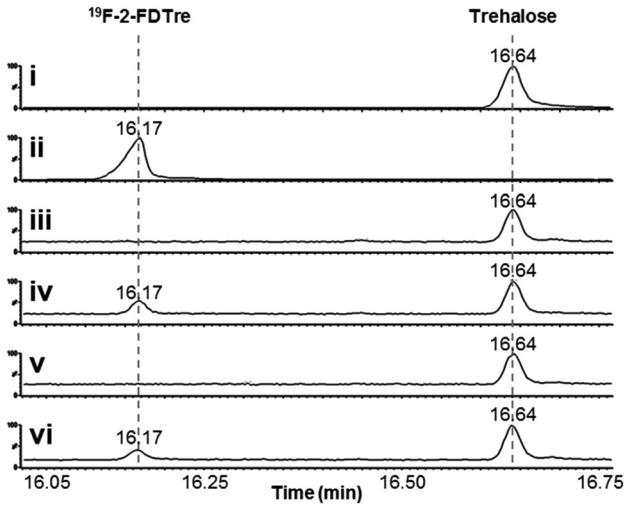


**Fig. 7** Representative GC-MS data demonstrating SugABC-LpqY-dependent uptake of $^{19}$F-2-FDTre (**9**) by *M. smegmatis*. Standards or cytosolic extracts from cells were dried, TMS-derivatized, and analyzed by GC-MS. (i) Trehalose standard; (ii) $^{19}$F-2-FDTre standard; (iii) untreated *M. smegmatis* wild type; (iv) $^{19}$F-2-FDTre-treated *M. smegmatis* wild type; (v) $^{19}$F-2-FDTre-treated *M. smegmatis* Δ*sugC* mutant; (vi) $^{19}$F-2-FDTre-treated *M. smegmatis* Δ*sugC*::*sugC* complement. See Fig. S3 in the ESI† for GC-MS data on other $^{19}$F-FDTre analogues.

tolerance at these positions, perhaps due to the disruption of a critical interaction (*e.g.*, hydrogen bond) at this region of the substrate. It has not yet been studied whether the homologous SugABC-LpqY transporters in pathogenic mycobacteria, such as *M. tuberculosis*, process FDTre analogues similarly to the *M. smegmatis* transporter. However, the consistency in TreAz uptake observed between *M. smegmatis* and *M. bovis* BCG[30]—a close genetic relative of *M. tuberculosis*—suggests that there may be overlap for at least a subset of the FDTre analogues. In sum, the considerable substrate tolerance of SugABC-LpqY, revealed by uptake experiments on the TreAz and FDTre series, provides justification for targeting this pathway with $^{18}$F-FDTre analogues for TB PET imaging applications.

### Protocol for the rapid synthesis, purification, and administration of $^{19}$F-2-FDTre to *M. smegmatis* as a model for future $^{18}$F-FDTre PET imaging applications

The data presented above indicate that TreT catalysis is ideally suited to the radiosynthesis of $^{18}$F-FDTre analogues. The ready availability of $^{18}$F-2-FDG at medical imaging facilities, coupled with the exceptionally high activity of TreT on this substrate, is of particular importance. We envision that TreT catalysis could be used in a radiosynthesis facility to convert freshly prepared $^{18}$F-2-FDG to $^{18}$F-2-FDTre, followed by product purification and administration to an *M. tuberculosis*-infected animal or human patient. To demonstrate the feasibility of this idea, we developed a protocol for $^{19}$F-2-FDTre production and utilization that models this process and can be executed in 1 hour.

In an effort to minimize FDTre preparation time, we shortened the reaction time and found that TreT could quantitatively convert $^{19}$F-2-FDG to $^{19}$F-2-FDTre in only 15 min at 70 °C. After the reaction was completed (15 min), the mixture was subjected to spin dialysis (10 min) followed by treatment with mixed-bed ion exchange resin (25 min). After passage through a 0.2 μm sterilization filter, an aqueous solution of pure $^{19}$F-2-FDTre of known concentration (approximately 5 mM‖) was in hand, and the entire process took only 1 hour. TLC and $^{1}$H NMR analysis of the $^{19}$F-2-FDTre product established its identity and purity (see Fig. S4A and S4B in the ESI†). Immediately after the filtration step, an appropriate volume of the $^{19}$F-2-FDTre solution was added to growing *M. smegmatis* strains (wild type, Δ*sugC* mutant, Δ*sugC*::*sugC* complement) to achieve a final concentration of approximately 25 μM. The cultures were incubated for 1 hour, then processed and analyzed by GC-MS as described above. The uptake results from this experiment were identical to those shown in Fig. 7 (see Fig. S4C in the ESI†).

These results demonstrate that the TreT method can be used to synthesize and purify $^{18}$F-FDTre analogues on a timescale that would still allow time to administer them to an animal or patient before the extinction of the radionuclide signal. This is especially significant considering that many hospitals already have the infrastructure both to synthesize $^{18}$F-2-FDG and image patients using PET, as it is often used to detect and monitor the treatment of cancer. Thus, our method could tap into existing medical infrastructure and expand its functionality to include imaging of TB patients.

## Conclusions

Most significantly, this study established an uncomplicated yet robust synthetic process for rapidly accessing FDTre analogues. The heat-stable glycosyltransferase TreT from *T. tenax* exhibited high activity on three out of four FDG substrates, which allowed their complete conversion to FDTre products in a matter of minutes—a favorable timescale for $^{18}$F-FDTre radiosynthesis. The expeditious purification protocol reported here is also fitting for radiosynthesis. Fortuitously, the FDTre product is the only neutral species in the TreT reaction mixture (as long as substrate conversion is quantitative), so purification was accomplished by a simple ion exchange step following enzyme removal. Also of benefit, the TreT synthesis process has a minimal environmental impact since it uses a single biocatalytic step and an entirely aqueous purification. At present, the scale of the TreT reaction is limited by the cost of UDP-glucose (~$300 g$^{-1}$), which we are currently working to address. Regardless, the reaction scale used in this study is more than sufficient for radiosynthesis applications. Because radiosynthesis is usually performed with small amounts of radioactive starting material, a future challenge will be to

‖The 5 mM concentration was estimated based on quantitative conversion of the substrate to product, which in this instance was confirmed by TLC and $^{1}$H NMR. Wash steps resulted in a four-fold dilution from the starting substrate concentration, which was 20 mM.

adapt the TreT reaction scale and stoichiometry to this setting. Also of note, 4-FDTre was not accessible *via* TreT catalysis and was instead chemically synthesized in this study. However, if 4-FDTre shows high promise for PET imaging applications, its radiosynthesis could potentially be accomplished by subjecting intermediate **18** to sequential trifluoromethanesulfonylation, $S_N2$ reaction with a [$^{18}$F]fluoride nucleophile, and deprotection.

FDTre analogues must emulate native trehalose to serve as probes for trehalose-related metabolic processes, which prompted us to investigate the effect of deoxyfluorination on the conformation of trehalose. Molecular mechanics predictions that deoxyfluorination would not distort trehalose's structure were corroborated by NMR analyses, which showed virtually no variability in intra- and inter-residue dihedral angles between trehalose and the FDTre analogues. Accordingly, FDTre analogues accurately mimic the conformation of trehalose, suggesting that they can potentially be used to probe trehalose metabolism in mycobacteria and other organisms.

An important potential application of $^{18}$F-FDTre analogues is *in vivo* PET imaging of *M. tuberculosis* infection. In support of this objective, it will be critical to thoroughly characterize the metabolism of FDTre analogues by mycobacteria. Here, we provided evidence that FDTre analogues were successfully recognized and taken up through the trehalose transporter SugABC-LpqY in whole *M. smegmatis* cells. Thus, the trehalose recycling pathway can serve as a biochemical sink through which FDTre analogues can accumulate in the cell. Further studies on FDTre uptake are warranted, including quantitation of SugABC-LpqY-mediated FDTre uptake in *M. smegmatis* and pathogenic mycobacteria, as well as uptake in other types of bacteria and mammalian cells to evaluate FDTre specificity for mycobacteria. In addition, the preliminary uptake experiments reported herein were conducted at micromolar concentrations to probe the transporter's substrate tolerance. Future studies should assess uptake efficiencies at FDTre concentrations that accurately reflect *in vivo* radiotracer concentrations. The possibility of Pks13, MmpL3, and Ag85 (and potentially other trehalose-processing proteins) being involved in the uptake of FDTre analogues should also be investigated.¶ The non-radioactive $^{19}$F-FDTre analogues reported herein will facilitate these experiments. Toward the long-term goal of this project, we are currently translating our results to the synthesis and evaluation of $^{18}$F-FDTre probes for PET imaging of mycobacterial infection in an animal model.

Finally, $^{18}$F-FDTre analogues may have applications beyond imaging mycobacterial infection. Many members of the gut microbiota use trehalose as a carbon source and osmoprotectant[62,63] and may metabolize $^{18}$F-FDTre, which could yield information on the dynamic changes that these bacteria undergo in response to diet, stress, and antibiotic treatment. It has also been proposed that trehalose may have value in treating neurodegenerative diseases due to its ability to prevent protein aggregation and induce autophagy.[64] $^{18}$F-FDTre analogues could be used to study the metabolic fate of trehalose in animals and confirm whether it accumulates in nervous tissue at concentrations high enough to counteract protein aggregation. Thus, $^{18}$F-FDTre analogues have the potential to impact various areas of biomedicine, and the methods established herein provide a platform for accessing this promising new class of nuclear imaging probes.

## Acknowledgements

This work was funded by a grant from the National Institutes of Health (R15 AI117670) to B. M. S. and P. J. W., as well as Cottrell College Scholar Awards from the Research Corporation to B. M. S. (22525) and P. J. W. (20185). L. M. M. was supported by a Provost's Fellowship from CMU. R. Kalscheuer is thanked for providing bacterial strains and L. Zhao is thanked for a critical reading of the manuscript.

## Notes and references

1 C. Dye, *Lancet*, 2006, **367**, 938–940.
2 A. Matteelli, A. Roggi and A. C. Carvalho, *Clin. Epidemiol.*, 2014, **6**, 111–118.
3 L. Norbis, P. Miotto, R. Alagna and D. M. Cirillo, *New Microbiol.*, 2013, **36**, 111–120.
4 World Health Organization, Global tuberculosis report 2015, 2015.
5 D. H. Johnson, L. E. Via, P. Kim, D. Laddy, C.-Y. Lau, E. A. Weinstein and S. Jain, *Nucl. Med. Biol.*, 2014, **41**, 777–784.
6 A. O. Ankrah, T. S. van der Werf, E. F. J. de Vries, R. A. J. O. Dierckx, M. M. Sathekge and A. W. J. M. Glaudemans, *Clin. Transl. Imaging*, 2016, **4**, 131–144.
7 L. Liu, Y. Xu, C. Shea, J. S. Fowler, J. M. Hooker and P. J. Tonge, *J. Med. Chem.*, 2010, **53**, 2882–2891.
8 E. A. Weinstein, L. Liu, A. A. Ordonez, H. Wang, J. M. Hooker, P. J. Tonge and S. K. Jain, *Antimicrob. Agents Chemother.*, 2012, **56**, 6284–6290.
9 X. Ning, W. Seo, S. Lee, K. Takemiya, M. Rafi, X. Feng, D. Weiss, X. Wang, L. Williams, V. M. Camp, M. Eugene, W. R. Taylor, M. Goodman and N. Murthy, *Angew. Chem., Int. Ed.*, 2014, **53**, 14096–14101.
10 G. Gowrishankar, M. Namavari, E. B. Jouannot, A. Hoehne, R. Reeves, J. Hardy and S. S. Gambhir, *PLoS One*, 2014, **9**, e107951.
11 E. A. Weinstein, A. A. Ordonez, V. P. DeMarco, A. M. Murawski, S. Pokkali, E. M. MacDonald, M. Klunk, R. C. Mease, M. G. Pomper and S. K. Jain, *Sci. Transl. Med.*, 2014, **6**, 259ra146.
12 S. L. Davis, N. A. Be, G. Lamichhane, S. Nimmagadda, M. G. Pomper, W. R. Bishai and S. K. Jain, *PLoS One*, 2009, **4**, e6297.
13 A. D. Elbein, Y. T. Pan, I. Pastuszak and D. Carroll, *Glycobiology*, 2003, **13**, 17R–27R.

 

14 H. Tournu, A. Fiori and P. Van Dijck, *PLoS Pathog.*, 2013, **9**, e1003447.
15 K. A. L. De Smet, A. Weston, I. N. Brown, D. B. Young and B. D. Robertson, *Microbiology*, 2000, **146**, 199–208.
16 P. J. Woodruff, B. L. Carlson, B. Siridechadilok, M. R. Pratt, R. H. Senaratne, J. D. Mougous, L. W. Riley, S. J. Williams and C. R. Bertozzi, *J. Biol. Chem.*, 2004, **279**, 28835–28843.
17 H. N. Murphy, G. R. Stewart, V. V. Mischenko, A. S. Apt, R. Harris, M. S. B. McAlister, P. C. Driscoll, D. B. Young and B. D. Robertson, *J. Biol. Chem.*, 2005, **280**, 14524–14529.
18 S. Gavalda, F. Bardou, F. Laval, C. Bon, W. Malaga, C. Chalut, C. Guilhot, L. Mourey, M. Daffé and A. Quémard, *Chem. Biol.*, 2014, **21**, 1660–1669.
19 A. E. Grzegorzewicz, H. Pham, V. A. K. B. Gundi, M. S. Scherman, E. J. North, T. Hess, V. Jones, V. Gruppo, S. E. M. Born, J. Kordulakova, S. S. Chavadi, C. Morisseau, A. J. Lenaerts, R. E. Lee, M. R. McNeil, M. Jackson, J. Korduláková, S. S. Chavadi, C. Morisseau, A. J. Lenaerts, R. E. Lee, M. R. McNeil and M. Jackson, *Nat. Chem. Biol.*, 2012, **8**, 334–341.
20 S. P. S. Rao, S. B. Lakshminarayana, R. R. Kondreddi, M. Herve, L. R. Camacho, P. Bifani, S. K. Kalapala, J. Jiricek, N. L. Ma, B. H. Tan, S. H. Ng, M. Nanjundappa, S. Ravindran, P. G. Seah, P. Thayalan, S. H. Lim, B. H. Lee, A. Goh, W. S. Barnes, Z. Chen, K. Gagaring, A. K. Chatterjee, K. Pethe, K. Kuhen, J. Walker, G. Feng, S. Babu, L. Zhang, F. Blasco, D. Beer, M. Weaver, V. Dartois, R. Glynne, T. Dick, P. W. Smith, T. T. Diagana and U. H. Manjunatha, *Sci. Transl. Med.*, 2013, **5**, 214ra168.
21 K. Tahlan, R. Wilson, D. B. Kastrinsky, K. Arora, V. Nair, E. Fischer, S. W. Barnes, J. R. Walker, D. Alland, C. E. Barry 3rd and H. I. Boshoff, *Antimicrob. Agents Chemother.*, 2012, **56**, 1797–1809.
22 N. Sathyamoorthy and K. Takayama, *J. Biol. Chem.*, 1987, **262**, 13417–13423.
23 J. T. Belisle, V. D. Vissa, T. Sievert, K. Takayama, P. J. Brennan and G. S. Besra, *Science*, 1997, **276**, 1420–1422.
24 K. M. Backus, M. A. Dolan, C. S. Barry, M. Joe, P. McPhie, H. I. Boshoff, T. L. Lowary, B. G. Davis and C. E. Barry 3rd, *J. Biol. Chem.*, 2014, **289**, 25041–25053.
25 R. Ryll, Y. Kumazawa and I. Yano, *Microbiol. Immunol.*, 2001, **45**, 801–811.
26 J. Indrigo, R. L. Hunter and J. K. Actor, *Microbiology*, 2003, **149**, 2049–2059.
27 E. Ishikawa, T. Ishikawa, Y. S. Morita, K. Toyonaga, H. Yamada, O. Takeuchi, T. Kinoshita, S. Akira, Y. Yoshikai and S. Yamasaki, *J. Exp. Med.*, 2009, **206**, 2879–2888.
28 R. Kalscheuer, B. Weinrick, U. Veeraraghavan, G. S. Besra and W. R. Jacobs, *Proc. Natl. Acad. Sci. U. S. A.*, 2010, **107**, 21761–21766.
29 K. M. Backus, H. I. Boshoff, C. S. Barry, O. Boutureira, M. K. Patel, F. D'Hooge, S. S. Lee, L. E. Via, K. Tahlan, C. E. Barry 3rd and B. G. Davis, *Nat. Chem. Biol.*, 2011, **7**, 228–235.
30 B. M. Swarts, C. M. Holsclaw, J. C. Jewett, M. Alber, D. M. Fox, M. S. Siegrist, J. A. Leary, R. Kalscheuer and C. R. Bertozzi, *J. Am. Chem. Soc.*, 2012, **134**, 16123–16126.
31 H. N. Foley, J. A. Stewart, H. W. Kavunja, S. R. Rundell and B. M. Swarts, *Angew. Chem., Int. Ed.*, 2016, **55**, 2053–2057.
32 V. A. Sarpe and S. S. Kulkarni, *Trends Carbohydr. Res.*, 2013, **5**, 8–33.
33 M. A. Chaube and S. S. Kulkarni, *Trends Carbohydr. Res.*, 2013, **4**, 1–19.
34 A. F. Hadfield, L. Hough and A. C. Richardson, *Carbohydr. Res.*, 1979, **71**, 95–102.
35 X. Li, H. Ohtake, H. Takahashi and S. Ikegami, *Tetrahedron*, 2001, **57**, 4297–4309.
36 R. Namme, T. Mitsugi, H. Takahashi and S. Ikegami, *Eur. J. Org. Chem.*, 2007, 3758–3764.
37 M. A. Rodriguez, O. Boutureira, M. I. Matheu, Y. Diaz, S. Castillon and P. H. Seeberger, *J. Org. Chem.*, 2007, **72**, 8998–9001.
38 M. Walmagh, R. Zhao and T. Desmet, *Int. J. Mol. Sci.*, 2015, **16**, 13729–13745.
39 P. Som, H. L. Atkins, D. Bandoypadhyay, J. S. Fowler, R. R. MacGregor, K. Matsui, Z. H. Oster, D. F. Sacker, C. Y. Shiue, H. Turner, C.-N. Wan, A. P. Wolf and S. V. Zabinski, *J. Nucl. Med.*, 1980, **21**, 670–675.
40 H. M. Giaever, O. B. Styrvold, I. Kaasen and A. R. Strøm, *J. Bacteriol.*, 1988, **170**, 2841–2849.
41 A. R. Strøm and I. Kaasen, *Mol. Microbiol.*, 1993, **8**, 205–210.
42 B. L. Urbanek, D. C. Wing, K. S. Haislop, C. J. Hamel, R. Kalscheuer, P. J. Woodruff and B. M. Swarts, *ChemBioChem*, 2014, **15**, 2066–2070.
43 T. Kouril, M. Zaparty, J. Marrero, H. Brinkmann and B. Siebers, *Arch. Microbiol.*, 2008, **190**, 355–369.
44 T. J. Tewson, M. J. Welch and M. E. Raichle, *J. Nucl. Med.*, 1978, **19**, 1339–1345.
45 T. R. Neal, W. C. Schumann, M. S. Berridge and B. R. Landau, *J. Labelled Compd. Radiopharm.*, 2005, **48**, 845–854.
46 R. W. Bassily, R. I. El-Sokkary, B. A. Silwanis, A. S. Nematalla and M. A. Nashed, *Carbohydr. Res.*, 1993, **239**, 197–207.
47 K. Bock, J. Defaye, H. Driguez and E. Bar-Guilloux, *Eur. J. Biochem.*, 1983, **131**, 595–600.
48 G. M. Brown, D. C. Rohrer, B. Berking, C. a. Beevers, R. O. Gould and R. Simpson, *Acta Crystallogr., Sect. B: Struct. Crystallogr. Cryst. Chem.*, 1972, **28**, 3145–3158.
49 G. A. Jeffrey and R. Nanni, *Carbohydr. Res.*, 1985, **137**, 21–30.
50 A. Moyano, C. A. Duda and E. S. Stevens, *J. Am. Chem. Soc.*, 1990, **112**, 7406–7407.
51 I. Tvaroška, M. Hricovíni and E. Petráková, *Carbohydr. Res.*, 1989, **189**, 359–362.
52 G. Batta, K. E. Kövér, J. Gervay, M. Hornyák and G. M. Roberts, *J. Am. Chem. Soc.*, 1997, **119**, 1336–1345.
53 A. Poveda, C. Vicent, S. Penades and J. Jiménez-Barbero, *Carbohydr. Res.*, 1997, **301**, 5–10.
54 N. W. H. Cheetham, P. Dasgupta and G. E. Ball, *Carbohydr. Res.*, 2003, **338**, 955–962.

55 M. K. Dowd, P. J. Reilly and A. D. French, *J. Comput. Chem.*, 1992, **13**, 102–114.
56 Q. Liu, R. K. Schmidt, B. Teo, P. A. Karplus and J. W. Brady, *J. Am. Chem. Soc.*, 1997, **119**, 7851–7862.
57 S. C. C. Nunesa, A. J. L. Jesus, M. J. Moreno and M. E. S. Eusébio, *Carbohydr. Res.*, 2010, **345**, 2048–2059.
58 F. L. Lin, H. van Halbeek and C. R. Bertozzi, *Carbohydr. Res.*, 2007, **342**, 2014–2030.
59 L. C. Lin, Ph.D. dissertation, University of California, Berkeley, 2006.
60 N. L. Allinger, Y. H. Yuh and J. H. Lii, *J. Am. Chem. Soc.*, 1989, **111**, 8551–8566.
61 V. V. Krishnamurthy, *J. Magn. Reson., Ser. A*, 1996, **121**, 33–41.
62 F. Peris-Bondia, A. Latorre, A. Artacho, A. Moya and G. D'Auria, *PLoS One*, 2011, **6**, e22448.
63 T. Duong, R. Barrangou, W. M. Russell and T. R. Klaenhammer, *Appl. Environ. Microbiol.*, 2006, **72**, 1218–1225.
64 E. Emanuele, *Curr. Drug Targets*, 2014, **15**, 551–557.